ICARUS **127,** 1–12 (1997)
ARTICLE NO. IS975681

Chaotic Diffusion and the Origin of Comets from the 2/3 Resonance in the Kuiper Belt

ALESSANDRO MORBIDELLI

Observatoire de la Côte d'Azur, B.P. 4229, 06304 Nice Cedex 4, France
E-mail: morby@obs-nice.fr

Received September 30, 1996; revised December 19, 1996

The dynamical structure of the 2/3 resonance at small inclination is explored using numerical integrations of test particles to compute the evolution of proper elements with time. The basic features are related to the analytically computed geography of secular resonances. This paper focuses on the existence of slowly diffusing chaotic orbits, which escape from the 2/3 resonance after billions of years. The origin of short-period comets may be related to the existence of such orbits. We numerically determine the rate at which 2/3 resonant objects are delivered to close encounters with Neptune. From this result we estimate the number of comet-sized objects that should presently be in the 2/3 resonance to explain the influx rate of observed short period comets; the result of 10^8 to 10^9 seems to imply that 2/3 resonant bodies should be collisionally evolved.

1. INTRODUCTION

The 2/3 mean motion resonance exterior to Neptune is probably the most interesting region in the Kuiper Belt; about 40% of the discovered objects seem to be located in the resonance. Although this number is exaggerated by observational biases, many of which favor the discovery of bodies in the 2/3 resonance, it is nevertheless certain that the resonance is heavily populated. In fact, it could be the dominant Kuiper Belt source of Jupiter family comets.

The dynamics in the 2/3 resonance have been already partially studied in a previous paper (Morbidelli *et al.* 1995). Using perturbation techniques we have shown that the secular dynamics within the 2/3 resonance are characterized mainly by the presence of the ν_{18} and Kozai resonances. The first of these is characterized by the corotation of the node of the body with the node of Neptune, and is responsible for large oscillations of the inclination; the second resonance concerns the libration of the argument of perihelion, and forces coupled oscillations of eccentricity and inclination. In Fig. 5 of Morbidelli *et al.* (1995) we have shown the location of both resonances on the e–i plane (for orbits with small amplitudes of libration in the 2/3 resonance). We have also confirmed the importance of these resonances through the numerical integration of both fictitious and "real" objects.

Duncan *et al.* 1995 showed numerically that in the 2/3 resonance there are orbits that are stable[1] for at least 4 byr. While this result was largely expected, an unexpected one was the discovery of several orbits that escape from the 2/3 resonance and encounter Neptune only after a very long time (>1 byr; this phenomenon also exists for other regions of the Kuiper Belt). The existence of these orbits is very important in understanding the origin of short-period (SP) comets. Indeed, since their dynamical lifetime is very short, the SP comets that we now observe must have left the Kuiper Belt just a few million years ago, many billions of years after their formation. Therefore, if one believes that the bodies in the Kuiper belt evolve only under the laws of dynamics (and do not suffer collisional "kicks," an assumption increasingly under discussion), then SP comets must come from orbits in the Kuiper belt that become unstable after billions of years, like those discovered by Duncan *et al.* (1995).

What is the nature of these orbits? What is the structure of the 2/3 resonance as far as long-term chaotic diffusion is concerned? In this paper we try to answer these two fundamental questions.

The only way to explore diffusive phenomena acting over billions of years is provided by numerical integrations; however, diffusive phenomena are usually hidden by large short-periodic oscillations, so that one must introduce some *proper elements* and compute their evolution with time. We explain our strategy in Section 2. In Section 3 we discuss our results and show which parts of the 2/3 resonance should be considered active sources of objects on a time scale of billions of years. In Section 4 we compare the numerical results with the analytically computed location of secular resonances. Secular resonances characterize

[1] Duncan *et al.* (1995) define an object to be stable if it does approach within a Hill sphere of Neptune.

0019-1035/97 $25.00

the main features of the dynamics in the 2/3 resonance: they generate strongly chaotic regions at large amplitudes of libration and are responsible for large oscillations of the inclination. Unfortunately analytical theories do not help us to understand the slow diffusion regions, since slow diffusion must be driven by very high order secular and secondary resonances which are beyond the limits of analytical approaches. In Section 5 we discuss the rate at which objects leave the 2/3 resonance and are delivered to Neptune. From this we estimate the order of magnitude of the number of comet-sized objects that should be presently in the 2/3 resonance to explain the observed number of SP comets.

2. DESIGN OF THE NUMERICAL INVESTIGATION

To achieve a global view of the dynamics in the 2/3 resonance, we integrate the evolution of 150 test particles over 4 byr, with initial conditions chosen as follows: the semimajor axis of all particles is set equal to the exact resonance value, i.e., $a_{\rm res} = 39.5$ AU; the critical angle of the mean motion resonance, namely,[2]

$$\sigma = -2\lambda_4 + 3\lambda - \tilde{\omega},$$

has been chosen randomly from 180° to 330°; the eccentricity and the inclination have been chosen randomly in the intervals [0, 0.3] and [0, 5°] respectively[3]; the longitude of perihelion $\tilde{\omega}$ and the longitude of node Ω have been randomly chosen in the range from 0° to 360°.

The choice of the range of values for σ needs elaboration. Neglecting all short-periodic and secular oscillations, for a given value of the eccentricity, the resonant phase space with respect to a and σ is as shown in Fig. 1; for $a = a_{\rm res}$ the initial value of σ determines the amplitude of libration in the resonance. In particular, $\sigma = 180°$ corresponds to the center of the resonance, namely, to the orbit with zero amplitude of libration; $\sigma = 360°$ corresponds to the border of the resonance, i.e., the separatrix. Moreover, the picture is symmetric with respect to $\sigma = 180°$, so that it is sufficient to choose initial conditions with $\sigma \geq 180°$. Thus, our choice of initial conditions allows us to cover the 2/3 resonance[4] (including coverage of the secular phases) up to $e = 0.3$ and $i = 5°$. This includes the region where most 2/3 resonant Kuiper belt objects are located (see the Minor Planet Center list) and is therefore the most interesting one.

[2] Here, λ and λ_4 denote the mean longitudes of the test particle and of Neptune, respectively, and $\tilde{\omega}$ is the particle's longitude of perihelion.

[3] The inclination is measured with respect to the invariable plane of the Solar System.

[4] In fact, short-periodic and secular oscillations force the libration center to move away from $a = a_{\rm res}$, $\sigma = 180°$. This decreases the probability of randomly choosing initial conditions corresponding to orbits with very small amplitude of libration.

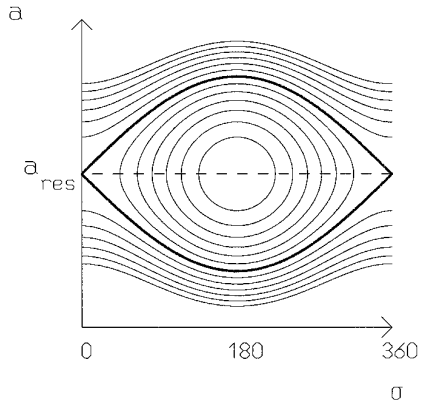

FIG. 1. Sketch of the dynamics of a mean-motion resonance in the averaged circular restricted three-body problem. The figure shows that, if the initial conditions are chosen on the line $a = a_{\rm res}$, the initial value of σ is related to the libration amplitude.

The goal of our numerical integration is to study possible diffusive phenomena and their relation to the existence of long-term escape trajectories from the 2/3 resonance. In this task we are confronted with two main problems: first, if we want to have good time resolution, the evolution of 150 particles over 4 byr would produce an unmanagably large numerical output; second, the oscillation of osculating elements would cover possibly genuine diffusive phenomena, since the latter are of much smaller amplitude. To overcome these two difficulties we compute on-line, numerically defined, proper elements for the test particles. Indeed, by definition, proper elements do not have oscillations and their changes are directly related to chaotic diffusion; moreover, since such changes are effective only on long time scales, it is enough to record one set of proper elements only every million years, therefore significantly reducing the size of the output file.

Proper elements can be defined and computed in several possible ways. The most accurate procedure is probably the use of digital filters (Carpino *et al.* 1987); however, here we use the simpler procedure of the so-called "supaction method," which seems to be accurate enough for our purposes. This method was first introduced by Laskar (1995) to analyze the results of a 15-byr integration of the planets, has been extensively studied by Froeschlé and Lega (1996) on several model maps, and has been already applied to the dynamics of small bodies in Morbidelli (1996). Briefly, the method relies on the following principle. Analyze a time-dependent signal with a running window; if the signal is quasi-periodic, the maxima (and the minima) assumed by the signal over each window are approximately the same (the accuracy improving with the amplitude of the analyzing window). Conversely, if the signal is not quasi-periodic, then the maxima (and the minima) will change from window to window. Now, if the

time-dependent signal is the evolution of the actions of a Hamiltonian dynamical system, the maxima (and the minima) computed on each window can be considered proper elements. Indeed, if the actions change quasi-periodically with time (i.e., the motion evolves on invariant tori), then the proper elements will not change, within the numerical accuracy of the method; conversely, if the system is slowly chaotic, the proper elements will still be free of the short-periodic oscillations but will change slowly, following the chaotic diffusion of the actions.

In the present case, the length of the analyzing running window was set equal to 10 myr, and proper elements were computed every million years. Therefore, the maximum and the minimum assumed by a, e, and i were computed on the intervals [0, 10] myr, [1, 11] myr, [2, 12] myr, etc.

As a check on the accuracy of such numerically defined proper elements, the same procedure was applied to compute the proper elements of Neptune, which can be considered a very good example of quasi-periodic evolution [chaotic diffusion of the outer planets, if it exists, must be smaller than the present limits of detectability; see Laskar (1990)]. Neptune's proper elements turn out to be very stable over the 4-byr integration: their rms deviation with respect to their average value was 8×10^{-4} AU for a, 1.2×10^{-4} for e, and 1.2×10^{-3} deg for i. Therefore, we can be confident that the proper elements of the test particles are accurate enough to study the structure of the 2/3 resonance and to point out the possible existence of both regular and slow chaotic orbits.

The integrations were performed using the swift_mvits program by Levison and Duncan (1994), which is based on the symplectic algorithm originally designed by Wisdom and Holman (1991). The integration includes the planets from Jupiter to Neptune. The stepsizes are 1y for Jupiter, 2y for Saturn, 4y for Uranus, and 8y for Neptune and the test particles.

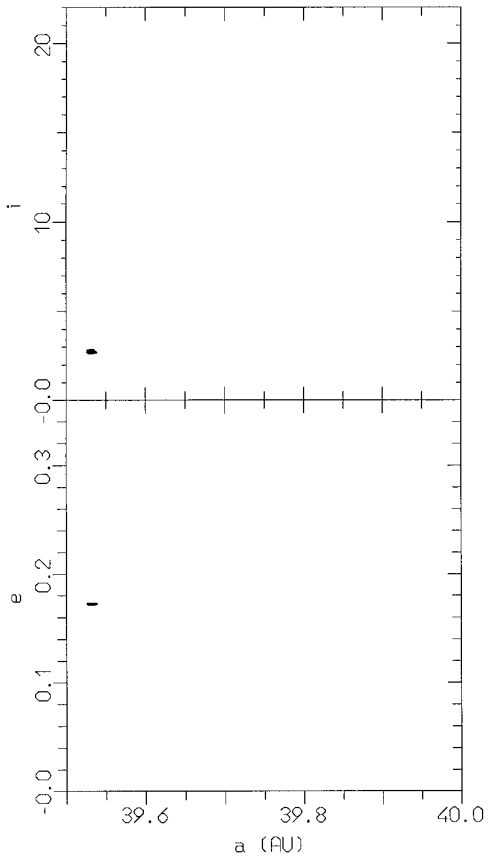

FIG. 2. Evolution of a regular orbit in the proper elements planes (a, i) (top) and (a, e) (bottom). Since the proper elements of regular orbits do not change significantly with time, the evolution over 4 byr results in a small spot (Class 1).

3. THE DYNAMICAL STRUCTURE OF THE 2/3 RESONANCE

Analyzing each of the 150 test particles' evolutions in the proper element space, we can identify four general classes of dynamical behavior. In Figs. 2 to 5 we show the evolution of one representative of each class in the plane of proper a–i (top) and proper a–e (bottom). The proper elements here are defined as the maxima of a, e, and i over the running window (see Section 2).

The first dynamical class is that of "regular orbits" (Fig. 2). As anticipated in the previous section, proper elements are constant for regular orbits, the osculating elements of which change quasi-periodically with time. Therefore, the evolution over 4 byr in the proper element space is simply a dot. Real regular orbits evolve on what the mathematicians call *invariant tori,* and will never escape from the 2/3 resonance. In practice, what we call here "regular orbits" are the orbits such that their chaotic diffusion, if it exists, is below the limits of detectability imposed by the finite accuracy of our proper elements method.

The second dynamical class is that of strongly chaotic orbits (Fig. 3). The proper elements change wildly with time (the arrows points to the initial condition); both the eccentricity and the inclination increase to large values. The orbit represented in Fig. 3 escapes the 2/3 resonance and encounters Neptune after *only* 420 myr.

The third dynamical class is that of long-term escapers (Fig. 4). These orbits are weakly chaotic and diffuse very slowly in the proper element space. More precisely, the proper eccentricity and inclination are almost constant, and the proper semimajor axis changes very slowly, diffusing in this case to a larger value. Such diffusion in semimajor axis denotes that the amplitude of libration in the 2/3 resonance is slowly increasing. Diffusing in the proper element space, these orbits finally dive into the strongly chaotic region. Then, as is the case in Fig. 3, the proper eccentricity and inclination change rapidly over a large region (note that

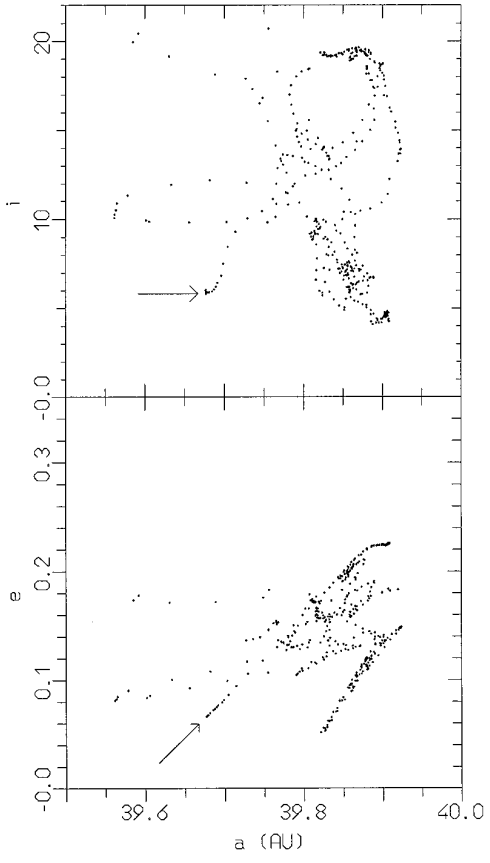

FIG. 3. Same as in Fig. 2, but for a strongly chaotic orbit. The proper elements change rapidly and over a large range, so that the points are very dispersed. This test particle encounters Neptune after 420 myr. The arrows point to the initial condition (Class 2).

the dots are dispersed). The orbit in Fig. 4 escapes the 2/3 resonance and encounters Neptune after 3.6 byr of integration (!!); more than 99% of this time is spent diffusing slowly to larger semimajor axis. We conjecture that all the long-term escapers found by Duncan *et al.* (1995) behave in this way. Note that this kind of behavior should not be an artifact of the numerical integration: indeed the code that we use is symplectic, so that it should not introduce artificial diffusions; moreover, the fact that we find, in the same integration, regular orbits that do not diffuse makes us confident that what we are observing here is a genuine dynamical phenomenon.

The fourth dynamical class is that of orbits that, although chaotically diffusing in the proper element space, do not escape the 2/3 resonance during the full integration time span (Fig. 5). These orbits have essentially the same nature as those in class 3, but, just by chance, do not escape: they spend part of the time diffusing toward smaller semimajor axis, namely, toward smaller amplitude of libration; therefore, they do not find their way to the strongly chaotic region. These orbits would probably escape the 2/3 on a longer integration time. Namely, extending the integration time span would allow several orbits to pass from class 4 to class 3.

We stress, moreover, that since we are dealing with a chaotic phenomenon, the outcome of diffusion is not deterministic. Therefore, integrating the same test particles with a different computer or with a different code, we would probably find several test particles originally identified in class 3 behaving as for class 4 and vice versa. Conversely, particles that belong to class 1 or class 2 in one numerical integration should still belong to the same classes in all other numerical experiments.

To obtain a global picture of the dynamical structure of the 2/3 resonance, we simultaneously plot together the evolutions of the 150 test particles. Figure 6 shows the resulting picture for the proper a–e plane; the colors denote the values of the proper inclination, to preserve the three-dimensional view of the phase space. We saw in Section 2 that we can define proper semimajor axis and eccentricity either as the maximum of a and e or as the minimum of

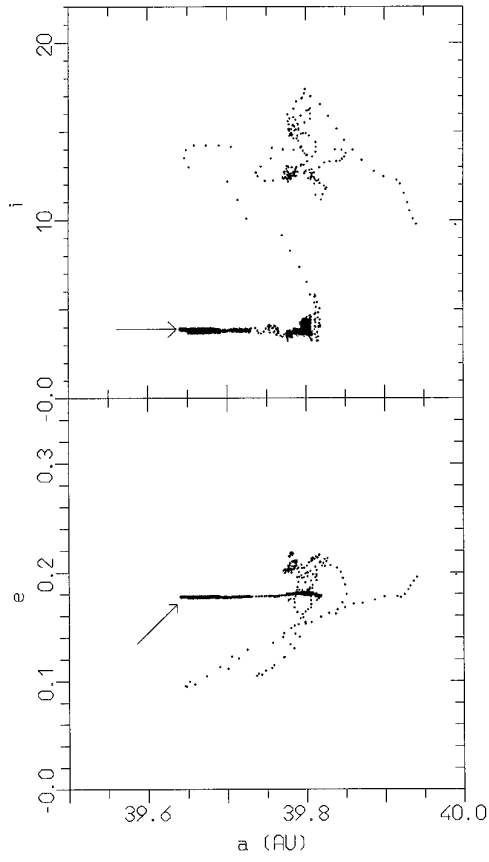

FIG. 4. Same as in Fig. 2, but for a slowly diffusing chaotic orbit. The arrows point to the initial condition. The proper semimajor axis changes very slowly, diffusing to larger values, and finally the test particle enters the strongly chaotic region where proper elements change quickly, as in Fig. 3. The particle encounters Neptune after 3.6 byr (Class 3).

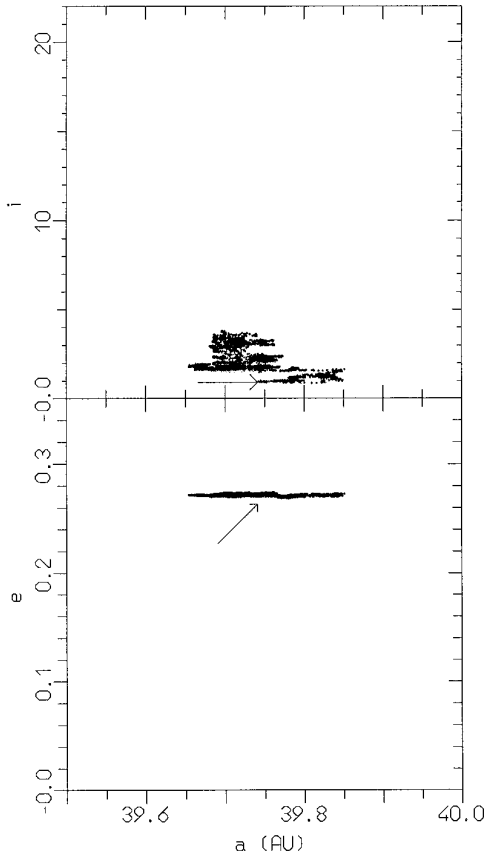

FIG. 5. Same as in Fig. 4 for another slowly diffusing orbit. In this case the particle does not encounter Neptune in 4 byr, since most of the time is spent diffusing to smaller proper semimajor axis (Class 4).

a and e over the running window; in Fig. 6 we plot both values.[5] As will be better explained in section 4, the two sets of proper elements correspond to the two sides of the resonance on the section $\sigma = 180°$. This is the reason why Fig. 6 shows a sort of symmetry with respect to $a \sim$ 39.5 AU, which is approximately the center of the resonance.[6] Moreover, in Fig. 6 we have performed some transformations to the two sets of proper elements to allow a direct comparison with the results of the analytic perturbation theory. Such transformations are explained in detail in Section 4.

Figure 6 can be considered a global chart of diffusion in the 2/3 resonance. Indeed, since proper elements are computed every million years, the regions where points accumulate correspond to the regions where the diffusion speed is smaller (the proper elements change slowly with time). Conversely, the regions where the points are more dispersed are the regions where the diffusion speed is larger and proper elements change quickly.

More precisely, Fig. 6 reveals that the 2/3 resonance has a well-defined structure. In the central part of the resonance (small libration amplitude) there are the regular stable orbits, which appear as small spots. We can easily recognize at least six such orbits, indicated by the arrows. The fact that proper elements do not diffuse with time, together with the fact that our choice of initial conditions disfavors small amplitudes of libration (as discussed earlier), makes the central part of Fig. 6 relatively empty of points.

Moving to larger semimajor axis (larger amplitude of libration), most of the traces of the evolution of the orbits are increasingly stretched; this reveals that these orbits are weakly chaotic and that the diffusion speed tends to increase with increasing semimajor axis. All these orbits, however, diffuse so slowly that they have no chance to escape from the 2/3 resonance within the age of the Solar System. At the end of the 4-byr integration time span, all of them are still well inside the resonance. No comets undergoing pure dynamical processes can come from this region.

Moving to larger semimajor axis, chaotic diffusion becomes more and more important. The traces of the orbits fuse together, densely filling a two-dimensional region. The blue and green colors show that the inclination does not increase to large values. All the orbits in this region have a chance to escape from the 2/3 resonance during the integration time, but only about 50% of them actually do in our experiment, with escape times ranging from 1.5 to 4 byr. As discussed in conjunction with Fig. 4, these are the orbits that happen to diffuse monotonically to larger proper a; conversely, the orbits that spend a significant fraction of time diffusing toward smaller proper a do not manage to escape, as illustrated by Fig. 5. Because of its dynamical properties, this region can be an active source of comets at the present age of the Solar System.

At still larger semimajor axis, close to the borders of the resonance, we find the strongly chaotic region where the dots are very dispersed since the proper elements change quickly. We have shown in Fig. 3 that the particles in this region have large inclination changes. This is confirmed here by the evident variety of colors: the maximal inclination reached by these orbits is 20°–25°. We show in Section 4 (Fig. 8) that the strong chaotic behavior in this region is determined by the interaction between the ν_{18} and Kozai resonances. The particles in this region have short dynamical lifetimes. All of them eventually encounter Neptune and, in our experiment, the region is completely depleted in 1.5 byr. Therefore this region should not be an active source of comets at present.

A final feature of the 2/3 resonance can also be observed in Fig. 6. At small eccentricity, all inclinations are pumped

[5] In both cases the color is associated with the proper inclination defined as the maximum of i over the running window.

[6] In the following we always refer for simplicity to the right part of the figure.

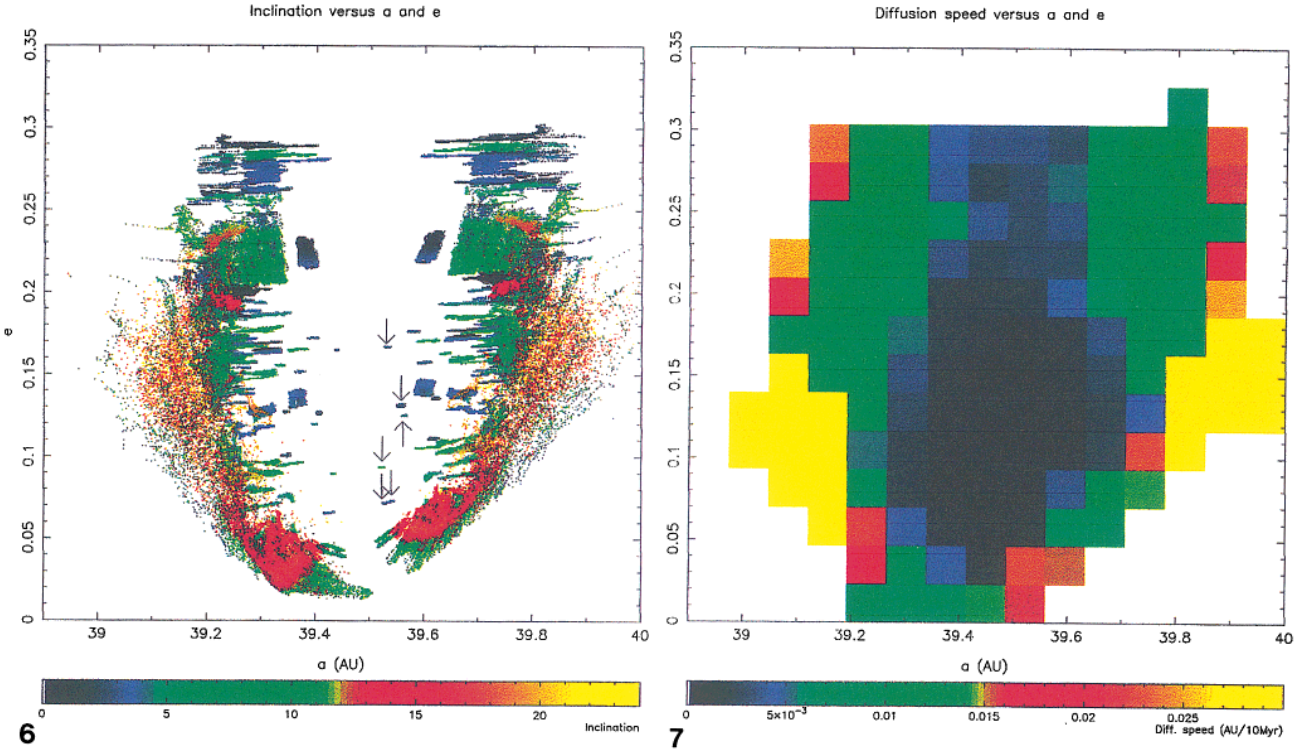

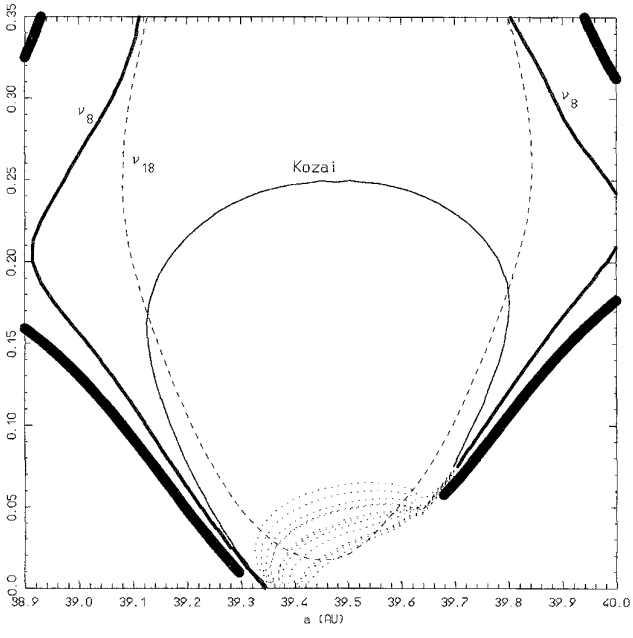

FIG. 6. Evolution of the proper elements of all 150 test particles. The color denotes the proper inclination. See text for comments.

FIG. 7. Map of diffusion speed in the 2/3 resonance. The color denotes the diffusion speed of the proper semimajor axis (measured in AU/10 myr). See text for comments.

FIG. 8. Location of the main secular resonances in the 2/3 commensurability with Neptune. The scale is the same as in Fig. 6, so that the two pictures can be directly compared (see Section 4.3 for discussion). The thick lines denote the borders of the resonance. Note that the resonance width shrinks at large eccentricity.

uniformly to about 15°; we show in Section 4 (Fig. 8) that this behavior is due to the presence of the ν_{18} resonance.

From Fig. 6 we now derive a quantitative map of diffusion speed. Divide the phase space into boxes and consider, one by one, all the points falling in each box. Each point corresponds to the proper elements that one test particle has at a certain time. Measure the difference Δa, Δe, Δi with the proper elements that the same test particle has 10 myr later. Do the same for all the points falling in the box and compute the average of the resulting values Δa, Δe, Δi; this gives the characteristic diffusion speed of the part of the phase space covered by the box. At the center of the resonance, where we have poor coverage in Fig. 6, some boxes turn out to be empty of points. For these boxes we estimate the diffusion speed by interpolating the values from the neighboring boxes.

Figure 7 shows the result concerning diffusion in semimajor axis Δa, the colors denoting the diffusion speed (measured in AU/10 Myr). Figure 7 confirms the radial structure of the dynamics in the 2/3 resonance. The regular orbits with negligible diffusion speed are at the center, and the diffusion speed increases as one moves outward to the borders of the resonance. The diffusion speed is also nonnegligible at small eccentricity ($e < 0.05$); note that the corresponding region in Fig. 6 is filled with points due to the slow diffusion of proper elements. We remark moreover that the black regular region shrinks as the eccentricity increases to 0.25.

4. THE GEOGRAPHY OF SECULAR RESONANCES

In this section we first explain a semianalytical perturbation approach to compute the location of secular resonances inside the 2/3 mean motion commensurability with Neptune. Then we discuss how to establish a relation between the numerically computed proper elements and the reference orbits used in the perturbation theory. Finally we return to Fig. 6 and discuss the relationship between the main features of the dynamical structure of the 2/3 resonance and the geography of the secular resonances.

4.1. Perturbation Theory and Secular Frequencies

To study the basic features of the secular dynamics in the 2/3 resonance we use the usual Hamiltonian formalism. The starting Hamiltonian is that of a massless body perturbed by the four giant planets, i.e.,

$$\mathcal{H} = -\frac{1}{2a} - \sum_{j=1,4} \mu_j \left(\frac{1}{|\mathbf{r} - \mathbf{r}_j|} - \frac{\mathbf{r} \cdot \mathbf{r}_j}{r_j^3} \right),$$

where $\mathbf{r}$ is the position of the massless body and $\mathbf{r}_j$ is the position of the jth perturbing planet with mass μ_j; the solar mass and the gravitational constant are taken to be unity. The planets are assumed to move on Keplerian orbits which undergo the secular changes described by the most recent theories of planetary motion (see, for instance, Nobili *et al.* 1989). Therefore the Hamiltonian is time dependent through the mean longitudes λ_j and the secular angles of the planets (which are all assumed to be linear functions of time). We extend the phase space introducing new actions Λ_j conjugate to λ_j.

To study the 2/3 resonance with Neptune we introduce the canonical variables

$$\begin{aligned}
&\sigma = -2\lambda_5 + 3\lambda - \tilde{\omega}, && S = L - G,\\
&\sigma_z = -2\lambda_4 + 3\lambda - \Omega, && S_z = G - H,\\
&\nu = -(-2\lambda_4 + 3\lambda), && N = \tfrac{2}{3}L - H,\\
&\lambda_4, && \Lambda_4' = \Lambda_4 + \tfrac{2}{3}L,\\
&\lambda_j, && \Lambda_j \ (j = 1, 2, 3),
\end{aligned}$$

where $L = \sqrt{a}$, $G = L\sqrt{1 - e^2}$, and $H = G \cos i$ are the actions conjugate to the mean anomaly l, the argument of perihelion ω, and the longitude of node Ω; the index ranges from 1 to 4, denoting the planets from Jupiter to Neptune. Recall that the longitude of perihelion is $\tilde{\omega} = \omega + \Omega$, and that the mean longitude is $\lambda = l + \tilde{\omega}$.

This choice of variables provides a well-defined separation between the fast and slow degrees of freedom. Indeed, in the 2/3 resonance, σ, σ_z, and ν are slow angles that do not move in the Keplerian approximation, while the mean longitudes of the planets $\lambda_1, \ldots, \lambda_4$ are fast angles.

As a first step, the Hamiltonian is averaged with respect to these fast angles. The averaging procedure would transform the Hamiltonian into an asymptotic series in powers of the planetary masses μ_j; for our purposes we just consider the terms linear in the masses. Technically, the average over λ_1, λ_2, and λ_3 is performed analytically, while the average over λ_4 needs to be computed numerically. Note, however, that the term that corresponds to the perturbation forced by the jth nonresonant planet ($j = 1, 2, 3$) depends, in the variables above, on both λ_j and λ_4 so that it must be doubly averaged, while the term corresponding to the perturbation forced by Neptune depends on λ_4 only.

We now split the averaged Hamiltonian into two parts: $\mathcal{H} = \mathcal{H}_0 + \mathcal{H}_1$. In $\mathcal{H}_0$ we place all the terms that are independent of σ_z, ν, and the planetary secular angles; $\mathcal{H}_1$ contains all the terms that average to zero with respect to the above angles. Using the D'Alembert characteristics, it is easy to see that $\mathcal{H}_1$ is at least proportional to the planetary eccentricities e' or inclinations i' or to the square of the inclination of the massless body. Therefore, since e' and i' are small and we are interested in orbits near the invariable plane (i small), $\mathcal{H}_1$ can be considered a perturbation of $\mathcal{H}_0$.

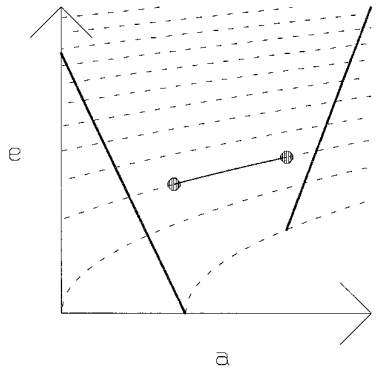

FIG. 9. Sketch of the evolution of (a, e) in the 2/3 resonance in the averaged circular problem. The two large dots denote the numerically computed proper elements and, in this case, correspond to the two sections of the reference orbit at $\sigma = 180°$. The future is computed on a plane S_z (=)constant and the dashed curves correspond to constant values of N.

The Hamiltonian $\mathscr{H}_0$ is integrable, since by construction it depends only on one angle, i.e., σ. It represents the best integrable approximation of the dynamics in the 2/3 resonance. Therefore, the orbits of $\mathscr{H}_0$ are hereafter called the *reference orbits.* Their evolution is very simple: they consist of a coupled oscillation in a and e, as shown in Fig. 9, while N and S_z are constant. Such oscillation is associated with the libration of σ around 180°: the larger the amplitude of libration of σ, the longer the trace of the reference orbit on the a–e plane. The alternate extremes of the oscillation in a and e are reached each time that $\sigma = 180°$. Therefore, on the section at $\sigma = 180°$, each reference orbit is represented by two large dots (Fig. 9), one on each side of the resonance. The two bold lines in Fig. 9 denote the limits of the maximal oscillation, corresponding to the maximum libration amplitude, for all possible values of N. These lines can therefore be considered the borders of the 2/3 resonance.

Since $\mathscr{H}_0$ is integrable, we can compute its frequencies. These are precisely the fundamental frequencies of the reference orbits. The first one is that of the periodic motion of the conjugated angle-action variables σ, S. To compute this frequency, we numerically integrate the equations of motion,

$$\dot{\sigma} = \frac{\partial \mathscr{H}_0}{\partial S}, \quad \dot{S} = -\frac{\partial \mathscr{H}_0}{\partial \sigma}, \tag{1}$$

up to the time T when the conditions $S(T) = S(0)$ and $\sigma(T) = \sigma(0)$ are both fulfilled. The time T is the period of the reference orbit under study, so that $2\pi/T$ is the first fundamental frequency.

The second and third fundamental frequencies (recall that the system has three degrees of freedom) are associated with the motion of the angles σ_z and ν. These are computed averaging $\dot{\sigma}_z$ and $\dot{\nu}$ over one period of the reference orbit, namely,

$$\langle \dot{\sigma}_z \rangle = \frac{1}{T}\int_0^T \frac{\partial \mathscr{H}_0}{\partial S_z}(\sigma(t), S(t), S_z, N)\, dt,$$

$$\langle \dot{\nu} \rangle = \frac{1}{T}\int_0^T \frac{\partial \mathscr{H}_0}{\partial N}(\sigma(t), S(t), S_z, N)\, dt.$$

Again, these frequencies are calculated with the aid of the computer. In these expressions $S(t)$ and $\sigma(t)$ are the numerically computed solutions of Eqs. (1), and the two integrals are computed using a procedure of numerical quadrature. It is worth remarking that, since the average frequency of σ is 0 (recall that σ librates), the fundamental frequencies $\langle \dot{\sigma}_z \rangle$ and $-\langle \dot{\nu} \rangle$ are precisely the secular frequencies of the argument of perihelion ω and of the longitude of perihelion $\tilde{\omega}$.

The location of secular resonances is then defined as the set of reference orbits with fundamental frequencies in rational commensurability with the planetary fundamental frequencies. For example, the ν_8 resonance is the 1:1 commensurability between $-\langle \dot{\nu} \rangle$ and the average frequency of Neptune's perihelion g_8; the ν_{18} resonance is the 1:1 commensurability between $-\langle \dot{\nu} \rangle - \langle \dot{\sigma}_z \rangle$ and the average frequency of Neptune's node s_8; the Kozai resonance corresponds to $\langle \dot{\sigma}_z \rangle = 0$; and so on. Since, as explained above, each reference orbit is represented by two dots on the section $\sigma = 180°$, we can use that section to plot the location of secular resonances as curves on the a–e plane. Figure 8 shows the result for $S_z = 0$, namely, on the invariable plane. Note the presence of three main secular resonances. The ν_8 resonance is present only at large eccentricity or large amplitude of libration. This is due to the fact that at small eccentricity and small libration amplitude the frequency of the longitude of perihelion is negative and of large absolute value (see Morbidelli *et al.* 1995). For the same reason, the secular resonances with the fundamental frequencies of the perihelia of the other giant planets are even at larger eccentricity, outside the region covered by Fig. 8. The Kozai resonance, conversely, cuts the center of the 2/3 commensurability at $e \sim 0.25$, and is therefore much more important for the motion of observed resonant objects. Finally, observe that the ν_{18} resonance is present at small eccentricity for small amplitude of libration. In the same region, several low-order secondary resonances can also be found: Fig. 8 plots by dotted curves the location of the resonances $2\pi/T + k(-\langle \dot{\nu} \rangle - g_8)$, $2\pi/T + k(-\langle \dot{\nu} \rangle - g_7)$, and $2\pi/T + K(-\langle \dot{\nu} \rangle - g_5)$ for $k = 1, \ldots, 5$ [the amplitudes of the g_6 terms are of negligible width in Neptune's spectrum so that the resonances $2\pi/T + k(-\langle \dot{\nu} \rangle - g_6)$ have not been plotted].

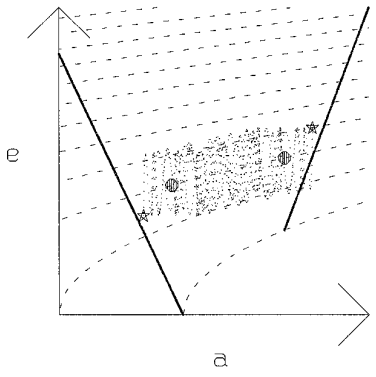

FIG. 10. Sketch of the evolution of (a, e) in the 2/3 resonance in the nonaveraged planar circular problem. The two stars denote the numerically computed proper elements, and the dots denote the two sections of the reference orbit at $\sigma = 180°$. The stars differ from the dots by an amount equal to the width of the short periodic oscillations of the osculating elements.

The effects of the perturbation $\mathscr{H}_1$ on $\mathscr{H}_0$ consist of secular changes in S_z, N, and of the amplitude of libration. These changes occur on a longer period than the motion along a reference orbit, so that in practice the motion in the complete system $\mathscr{H}_0 + \mathscr{H}_1$ passes slowly from one reference orbit to another. The effects of $\mathscr{H}_1$ are magnified in the presence of resonances. The ν_8 resonance forces large changes of N, the Kozai resonance forces large changes of S_z, and the ν_{18} resonance forces large coupled changes of N and S_z (with $N - S_z$ remaining almost constant).

4.2. Relationship between Proper Elements and Reference Orbits

We now discuss the relationship between the numerically computed proper elements (defined in Section 2) and the reference orbits, which are at the basis of the analytical computation of the location of secular resonances. For this purpose, we consider the following gradual complication of the equations of motion and the corresponding meanings of the proper elements.

Start with the simplest set of equations, namely, those of the averaged planar circular restricted problem with Hamiltonian $\mathscr{H}_0$. In this case the relationship is straightforward: the numerically computed proper elements give exactly the two large dots in Fig. 9, i.e., the sections of the reference orbit with $\sigma = 180°$.

Consider now the nonaveraged equations of the planar circular restricted problem. In this case, the osculating a and e have short-periodic oscillations around the corresponding mean elements, which evolve along a reference orbit. The evolution on the a–e plane looks like that of Fig. 10. The numerically computed proper elements correspond to the two stars in Fig. 10, which are shifted with respect to the large dots by a quantity (da, de), which is precisely the half-width of short-periodic oscillations. Therefore, to establish the relationship with the reference orbit, we have to measure the half-width of short-periodic oscillations and to add it to (subtract it from) the values of proper elements. This calibration eliminates the effect of short-periodic oscillations on the definition of proper elements, as if we were dealing with the averaged problem.

Consider now the full averaged problem $\mathscr{H}_0 + \mathscr{H}_1$. The effect of $\mathscr{H}_1$ is to force secular long-periodic oscillations of the actions N and S_z and, possibly, chaotic diffusion. Consider only long-periodic oscillations. In this case, the evolution on the a–e plane looks like Fig. 11: the reference orbit changes slowly, oscillating between two N levels. If the analyzing running window is longer than the period of secular oscillations, the numerically computed proper elements give the values corresponding to the two squares in Fig. 11. A simple, approximate relationship with the dots representing the mean reference orbit is provided by what we call the "N algorithm," which can be expressed as follows. Denote by (a_1, e_1) and (a_2, e_2) the coordinates of the two dots; compute the values $N_{\min}$ and $N_{\max}$ associated respectively with the couples of proper elements $(a_{\min}, e_{\min})$ and $(a_{\max}, e_{\max})$ and define $\overline{N} = (N_{\min} + N_{\max})/2$. Then a_1 and a_2 are approximately equal to $a_{\min}$ and $a_{\max}$, respectively, and e_1 and e_2 are such that their corresponding N levels are equal to $\overline{N}$.

Let us now return to our numerical integrations of fictitious particles in the 2/3 resonance. Since we integrate the full equations of motion, in the numerically computed proper elements $[a_m(t), e_m(t)]$ and $[a_M(t), e_M(t)]$, we have the effects of both the short-periodic oscillations and the secular oscillations forced by $\mathscr{H}_1$. So, we have first per-

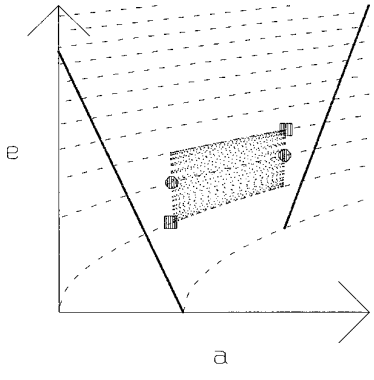

FIG. 11. Sketch of the evolution of (a, e) in the 2/3 resonance in the averaged elliptic problem. The two squares denote the numerically computed proper elements. The relation with the dots, denoting the sections of the reference orbit at $\sigma = 180°$, is given by the N algorithm discussed in the text.

formed an integration over a time span of 1 myr with output every integration time step, and have used this integration to measure, for each test particle, the amplitude of the short-periodic oscillations (da, de). This amplitude has been added to/subtracted from the full time series of proper elements, producing for each particle a time series of calibrated proper elements $[a_{\min}(t), e_{\min}(t)]$ and $[a_{\max}(t), e_{\max}(t)]$, where $a_{\min}(t) = a_{\rm m}(t) + da$, $e_{\min}(t) = e_{\rm m}(t) + de$, $a_{\max}(t) = a_{\rm M}(t) - da$, and $e_{\max}(t) = e_{\rm M}(t) - de$. Finally, we have applied the N algorithm to such series of calibrated proper elements, thus obtaining the time series of $[a_1(t), e_1(t)]$ and $[a_2(t), e_2(t)]$. Figure 6 is the outcome of all these transformations, plotting $[a_1(t), e_1(t)]$ and $[a_2(t), e_2(t)]$ for all the test particles and, therefore, can be directly compared with Fig. 8.

4.3. Secular Resonances and Diffusion in the 2/3 Resonance

We finally come to the comparison of Figs. 6 and 8.

A first remarkable feature is that the large increase in inclination, which characterizes the red regions at the bottom of Fig. 6, corresponds to the location of the ν_{18} resonance, as plotted in Fig. 8; however, the secular resonance alone does not explain why the proper elements diffuse slowly on the a–e plane. This is probably due to the interaction with low-order secondary resonances, which, as shown in Fig. 8, are present in large number in that region.

The effects of the Kozai resonance are not well visible. This is due to the fact that the strength of the Kozai resonance increases with the inclination, while all the test particles considered in this paper have a small initial i. There are no Pluto-like orbits in the present work.

The strong chaotic region at large amplitude of libration in Fig. 6 seems to be due to the interaction between the ν_{18} and Kozai resonances, which in Fig. 8 appears to be very close for the corresponding part of the diagram.

In Fig. 6 no dots are visible in the large-amplitude libration region characterized by the location of the ν_8 resonance. This indicates that the region is so violently unstable that the typical lifetime is smaller than the length of the analyzing running window for the computation of proper elements (10 myr). This is not surprising since the ν_8 resonance acts on the eccentricity, and large changes in the eccentricity force the particles to be ejected from the 2/3 resonance (since the resonance shrinks at both larger and smaller e), thus losing the resonant protection mechanism and encountering Neptune.

Conversely, no low-order secular or secondary resonance seems to explain the slow diffusion region, which would be the active source of comets at the present age of the Solar System. Such slow diffusions should be due to very weak chaos generated by secular or secondary resonances of very high order. We could always find some high-order resonances located in that region, since resonances are dense, but the investigation of their effects goes beyond the limits of perturbation analysis.

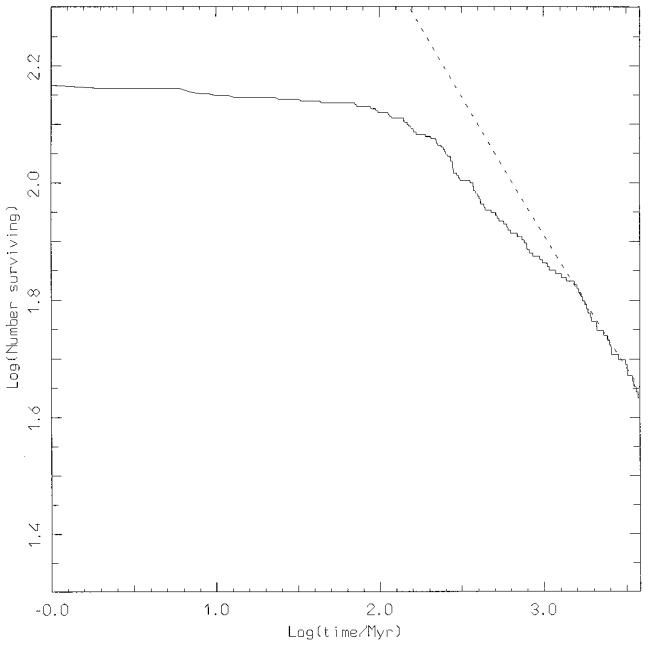

FIG. 12. Evolution of the number of surviving particles N as a function of time t. The dashed line shows a fit to the last portion of the plot, with slope $-1/2$.

5. ORIGIN OF COMETS FROM THE 2/3 RESONANCE

From our numerical experiment, we can try to derive a delivery rate of 2/3 resonant bodies to Neptune. Figure 12 shows the logarithm of the number of the surviving particles N as a function of logarithm of time. The derivative of this function is precisely the delivery rate. Recall that a body is considered dead when it encounters Neptune within 1 Hill sphere, so that the surviving bodies are those that never encounter the planet.

It can be seen that the curve has at least two changes of slope. The first one is at about 100 myr and probably corresponds to the time when the strongly chaotic region starts to be an efficient source of Neptune crossers. The second change of slope is at about 1.5 byr: this is the time when the strongly chaotic region is completely depleted and the slow chaotic region starts to be the dominant source of Neptune-encountering bodies.

The slope for $t > 1.5$ byr is approximately 0.5, which suggests a relation for the number of surviving particles N at time t of type $N(t) = A + B/\sqrt{t}$. Nevertheless, since the time interval is quite limited, functions like $N(t) = A - B \log(t)$ (suggested by Holman and Wisdom 1993), and

$N(t) = A + B/\log(t)$ [found by Simó *et al.* (1995) in a similar numerical experiment; see also the conclusions in Morbidelli *et al.* (1995)] also produce a satisfactory fit to the results; however, we know from the detailed analysis of the dynamical behavior of the test particles that we have in our experiment six particles on invariant tori, which would never escape the 2/3 resonance. This fixes the limit $t \to +\infty$ of the distribution $N(t)$, namely, the parameter A. Of the three tentative relations indicated above, only $N(t) = 6 + 2390/\sqrt{t}$ turns out to be an acceptable fit. Therefore, consider

$$\frac{dN}{dt} = -\frac{N_0}{t^{3/2}}, \tag{2}$$

where N_0 is a constant related to the number of particles, as the delivery rate of 2/3 resonant bodies to Neptune.

We have a theoretical interpretation of this relation. Section 3 pointed out that chaotic diffusion is essentially a one-dimensional process, since it acts mainly on the libration amplitude. Moreover, at the center of the resonance there are invariant tori, and the diffusion speed increases with the amplitude of libration up to the strongly chaotic region. On the other hand, it is known from the general theory of Hamiltonian systems that the diffusion speed in the vicinity of an invariant torus depends on the distance d from the torus. More precisely, it is superexponentially slow ($\sim 1/\exp[\exp(1/d)]$), up to some threshold distance, then exponentially slow ($\sim 1/\exp(1/d)$) up to a further threshold distance, then quadratically slow ($\sim d^2$) up to a final threshold, which usually marks the transition to strong chaos (Morbidelli and Giorgilli, 1994). A one-dimensional random walk model, with step amplitude proportional to d^2, gives exactly a delivery law of the form $dN/dt \sim -1/t^{(3/2)}$ (Morbidelli and Vergassola 1996). Therefore we interpret the observed delivery rate from the 2/3 resonance as the trace of a dynamical structure characterized, under the influence of invariant tori, by a diffusion speed increasing as the square of the libration amplitude.

We now estimate how many comet-sized bodies must presently be in the 2/3 resonance to supply the observed flux of short-periodic comets in the inner Solar System. Duncan *et al.* (1995) estimated that such flux implies that 2×10^8 comet-sized bodies encounter Neptune per billion years. Since we know that about 40% of the discovered bodies in the inner Kuiper belt are in the 2/3 resonance, we can expect that, within a factor 3, 25% of this input comes from the 2/3 resonance, namely, 5×10^7 bodies per billion years. We now assume that the bodies evolve only under the laws of dynamics, without suffering kicks due to collisions and close encounters that could replace them in the phase space. In this case, all bodies escaping the 2/3 resonance and encountering Neptune do so solely under the effect of chaotic diffusion, as in our numerical experiment. According to our numerical integration, the slow diffusion region is the only active source of the 2/3 resonance producing Neptune-encountering bodies at the present epoch of the Solar System. More precisely, from a population of 50 bodies initially in this region, we find that 5 bodies are delivered to Neptune in the last billion years. Therefore there would have originally been 5×10^8 bodies in the slow chaotic region in the 2/3 resonance. About 50% of these bodies would still be there (recall that in the integration only 50% of the test particles in the slow chaotic region actually encounter Neptune in 4 byr). Finally, we also have to take into account the population of bodies that are in the inactive regions of the 2/3 resonance. From our data, we compute that the volume of the region where bodies are either on invariant tori or on orbits with diffusion speed too slow to escape from the 2/3 resonance over the age of the Solar System is about 40% of the volume of the slow diffusion region. Therefore, the number of bodies presently in the 2/3 resonance should be of order of

$$N_{\text{now}} = N_{\text{active}} + N_{\text{inactive}} = \frac{5 \times 10^8}{2} + 0.4 \cdot 5 \times 10^8 = 4.5 \times 10^8.$$

This number is consistent with the ones estimated for the inner Kuiper Belt by Cochran *et al.* (1995) ($\sim 10^8$) and by Duncan *et al.* (1995) (5×10^9). It has been already shown (Davis and Farinella 1996) that these numbers imply that the Kuiper Belt bodies should be collisionally evolved. Therefore our original assumption must be wrong: bodies can also be delivered to Neptune by being ejected directly from the regular regions in the 2/3 resonance by collisions or by close encounters with bodies of size comparable to 1992 QB_1. The real dynamics in the 2/3 resonance with Neptune is driven by a combination of chaotic diffusion and collisional kicks.

6. CONCLUSIONS

In this paper we have shown that the 2/3 resonance with Neptune has a complex dynamical structure. The ν_{18} resonance pumps the inclination at small eccentricity. Regular orbits are present only at moderate eccentricity and small amplitude of libration. At large amplitude of libration, the interaction between the ν_{18} and Kozai resonances generates a strongly chaotic region, which is quickly depleted. The transition region at moderate amplitude of libration is characterized by slow chaotic diffusion. This region should be an active source of Neptune-encountering bodies at the present age of the Solar System. From the delivery rate that has been determined, we have computed the number of comet-sized objects that should presently be in the 2/3 resonance to explain the observed flux of short-period comets in the inner Solar System. This number turns out to be about 4.5×10^8, and seems to indicate

that the 2/3 resonant bodies must still be under collisional evolution. Therefore, comets must be ejected from the 2/3 resonance by a combination of chaotic diffusion and collisional ''kicks.''

In this paper we discussed how to define and compute suitably accurate proper elements, which are of fundamental importance in exploring the phenomena of slow chaotic diffusion and allow one to extract as much information as possible from the numerical integrations. Moreover, we have shown how to relate the numerical results with the analytical picture of the location of secular resonances.

ACKNOWLEDGMENTS

I thank M. Moons for all her suggestions and remarks and for her help in the implementation of the perturbation approach leading to the geography of secular resonances. I am in debt to B. Gladman for useful discussions and a careful reading of my manuscript. I also thank J. M. Petit for his help with the color graphics software.

REFERENCES

Carpino, M., A. Milani, and A. Nobili 1987. Long-term numerical integrations and synthetic theories for the motion of the outer planets. *Astron. Astrophys.* **181,** 182–194.

Cochran, A. L., H. F. Levison, S. A. Stern, and M. J. Duncan 1995. The discovery of Halley sized Kuiper belt objects using the Hubble Space Telescope. *Astrophys. J.* **455,** 342–346

Davis, D. R., and P. Farinella 1996. Collisional evolution of Edgeworth Kuiper Belt objects. *Icarus* **125,** 50–60.

Duncan, M. J., H. F. Levison, and S. M. Budd 1995. The dynamical structure of the Kuiper Belt. *Astron. J.* **110,** 3073–3081.

Froeschlé, C., and E. Lega 1996. On the measure of the structure around the last KAM torus before and after its break-up. *Celest. Mech. Dynam. Astron.,* in press.

Holman M. J., and J. Wisdom J. 1993. Stability of test particle orbits in the outer Solar System. *Astron. J.* **105,** 1987–1999.

Laskar J. 1990. The chaotic motion of the solar system: A numerical estimate of the size of the chaotic zones. *Icarus,* **88,** 266–291.

Laskar, J. 1995. Large scale chaos and marginal stability in the Solar System. *XIth ICMP Colloquium,* Paris.

Levison, H. F., and M. J. Duncan 1994. The long-term dynamical behavior of short period comets. *Icarus* **108,** 18–36.

Morbidelli, A. 1996. On the Kirkwood gap at the 2/1 commensurability with Jupiter: Numerical results. *Astron. J.* **111,** 2453–2461.

Morbidelli, A., and A. Giorgilli 1994. Superexponential stability of KAM tori. *J. Stat. Phys.* **78,** 1607–1617.

Morbidelli, A., and M. Vergassola 1996. Escape rates in Hamiltonian systems. *J. Stat. Phys.,* submitted.

Morbidelli, A., F. Thomas, and M. Moons 1995. The resonant structure of the Kuiper belt and the dynamics of the first five trans-neptunian objects. *Icarus* **118,** 322–340.

Nobili, A., A. Milani, and M. Carpino 1989. Fundamental frequencies and small divisors in the orbits of the outer planets. *Astron. Astrophys.* **210,** 313–336.

Simó, C., G. Gómez, A. Jorba, and J. Masdemont 1995. The bicircular problem near the triangular libration points in the RTBP. In *From Newton to Chaos* (A. E. Roy and B. A. Steves, Eds.). Plenum, New York.

Wisdom, J., and M. J. Holman 1991. Symplectic maps for the *N*-body problem. *Astron. J.* **102,** 1528–1538.